Many thanks for the detailed correction of all typos and inconsistencies that were still present in the text. We have closely followed your recommendations to include the major and minor changes you have recommended and to restructure parts of the manuscript accordingly.

In this regard, we have revised and rewritten a few sections such as Abstract, method, results, discussion and conclusion in the revised manuscript. Quality control and revision of dissipation estimates, as well as current calculations were also done to ensure the validity of our results. We thought it useful to point out its detailed revisions (lines and sections) in the replies to your comments. Below (highlighted in blue and magenta) is an itemized response to the different issues raised in the review.
We believe that with all these additional changes and thanks to your valuable suggestions, we have achieved a marked improvement in the readability of the manuscript, as well as in the formal presentation and description of its main findings.

This paper reports on microstructure measurements off the Amazon shelf. This is an interesting area with a combination of various dynamical processes, internal tides, low frequency circulation and amazonian water lenses. Consistently with this dynamics contrasted dissipation rates are observed with the highest values at generation sites, and along internal tide pathways and the lowest values in no-tidal areas. The relative contribution to dissipation of the mean baroclinic current (North Brazil current) compared to that of internal tide was estimated : the contribution of IT shear was found larger than BC shear near generation sites, equal along IT pathways. In addition turbulent diffusive nutrient fluxes were computed : large values were obtained.

I think there is interesting material for publication but that part of the analysis must be revisited to provide convincing results before it could be accepted for publication. Some of the figures are overloaded and not easily readable, having many figures in the appendix does not facilitate a fluent reading. Part of the sections would need a careful polishing.

The main result to highlight is the spatial contrast of dissipation rates and give insights on the origin of these variations.

I list in the following my main general comments:

-More information on the background state should be given: bathymetry, sea surface salinity (Amazone plume), as well as the mean current and for instance information on generation sites for internal tides (reorganization of Figure 1 which is not easy to read, subplot (b) does not seem necessary)

R:Thank you for your comment.

We have updated the information on the background state, including bathymetry, the Amazon plume, internal tide generation sites, and mean circulation, and reorganized Figure 1 of the manuscript accordingly.

Revisions can be found in the "Introduction" section, lines 34-82, and the updated Figure 1 of the revised manuscript is provided below. We retained Figure 1b of the manuscript as it highlights the signature of the ISWs observed in the region during the AMAZOMIX cruise.

The revisions are shown below:

“

1 Introduction

Turbulent mixing in the ocean plays an important role in sustaining the thermohaline and meridional overturning circulation and in closing the global ocean energy budget (Kunze, 2017). These processes have strong implications for the climate, influencing heat and carbon transport, as well as nutrients supply for photosynthesis (Huthnance, 1995; Munk and Wunsch, 1998). Mixing processes can result from wind in the surface waters layer, internal waves and shear instability in the ocean interior, and bottom friction near the bottom layer (Miles, 1961; Thorpe, 2018; Ivey et al., 2020; Inall et al., 2021). Barotropic tides interacting with steep shelf-break topography trigger internal waves at tidal frequencies and harmonics, known as internal tides (ITs), which can propagate and produce mixing. These ITs can be expressed by large vertical displacements (up to tens of meters) of water masses (Garrett and Kunze, 2007). After their generation on the shelf-break, the (more unstable) higher modes of ITs may dissipate locally, while the lower modes can propagate far away (Zhao et al., 2016). IT beams (generated where the slope of the ITs and the topography match together on the shelf-break) can propagate vertically, resulting in reflection, scattering and dissipation of ITs at the bottom, surface waters, or thermocline levels (New and Da Silva, 2002; Gerkema and Zimmerman, 2008; Bordois, 2015; Zhao et al. 2016). They can also dissipate when energy fluxes interfere (Zhao et al., 2012) or interact with strong baroclinic eddies or currents (Rainville and Pinkel, 2006; Whalen et al., 2012). Furthermore, ITs may disintegrate into packets of higher-mode nonlinear internal solitary waves (ISWs), which can propagate and dissipate offshore (Jackson et al., 2012).

Previous and recent studies have shown that ITs-induced turbulent mixing can affect the surface, such as sea surface temperature (Ray and Susanto, 2016; Nugroho et al., 2018; Assene et al., 2024), chlorophyll content (Muacho et al., 2014; M’Hamdi et al., 2024; in preparation), marine ecosystems (Wang et al., 2007; Zaron et al., 2023), and atmospheric convection and the rainfall structure (Koch-Larrouy et al., 2010, Sprintall et al. 2014).

In the western tropical Atlantic, the Amazon River-Ocean Continuum (AROC) constitutes a key region of the global oceanic and climate system (Araujo et al., 2017; Varona et al., 2018). This region (Fig. 1a) is characterized by a system of western boundary currents, including North Brazil Current (NBC). NBC, which flows northwestward, has its core velocities (~ 1.2 m s^{-1}) that remain stable from the surface to a depth of 100 m (Johns et al., 1998; Bourlès et al., 1999; Barnier et al., 2001; Neto and Silva, 2014). This region also experiences highly variable dynamics due to the Amazon River Plume. During the rainy season (May-July), peak discharge can extend the plume over 1500 km offshore, northwest along the NBC. In the dry season

(September-November), reduced discharge and stronger saline intrusion may confine the plume to less than 500 km offshore, near the Amazon Shelf, with some eastward dispersion (Coles et al., 2013). The Amazon plume can generate vertical shear in underlying currents, enhancing mixing. Additionally, a system of Amazonian Lenses of water (AWL), influenced by continental inputs, may affect both the boundary layer and mixed layer patterns (Silva et al., 2005; Prestes et al., 2018).

In the AROC region, the Amazon shelf-break is a hotspot for the generation, propagation and dissipation of ITs and ISWs as a result of non-linear processes (Geyer, 1995; Brandt et al., 2002; Magalhães et al., 2016; Ruault et al., 2020; Tchilibou et al., 2022; Fig 1). Previous studies using Synthetic Aperture Radar (SAR) satellite images (Magalhaes et al., 2016) identified ISWs along the path of ITs propagating from two sites (i.e., sites Aa and Ab; Fig. 1a). Conversely, other sites showed no ISWs propagation (i.e., sites E and D; Fig. 1a, 1b and 1c) (see Magalhaes et al., 2016 for definition). Using numerical modeling, Tchilibou et al. (2022) showed that about 30 % of the M2 (dominant tidal component; Le Bars et al. 2010) ITs energy is dissipated locally (for higher-modes ITs) at sites E, Aa, Ab and D (Fig. 1a), while the remaining lower-modes ITs energy can be dissipated remotely. Dissipation away from the generation sites (E, Aa, Ab and D; Fig. 1a) can result from the shear instabilities caused by ITs-ITs and/or ITseddy/current interactions. Despite the presence of ITs, no direct measurements of dissipation rates have been conducted to our knowledge.

The mixing induced by these internal waves in the region was observed during the AMAZOMIX cruise (Bertrand et al., 2021). The cruise was designed with stations/transects inside and outside ITs fields (Fig. 1a and 1c) to measure ITs dissipation and study their impact on the AROC ecosystem. Direct microstructure measurements of temperature, salinity and velocity were conducted at the different repeated stations/transects over a M2 tidal cycle (~ 12.42 h). These cruise measurements offer an opportunity to explore whether ITs play a role in mixing within the AROC region. In this study, we will quantify mixing and identify the associated processes off the Amazon shelf. We will calculate turbulent kinetic energy (TKE) dissipation rates, vertical displacements of isopycnal surfaces and vertical eddy diffusivities using in situ microstructure and hydrography data. Finally, the baroclinic shear of currents and their contributions to mixing will be calculated from current data collected between stations and transects.

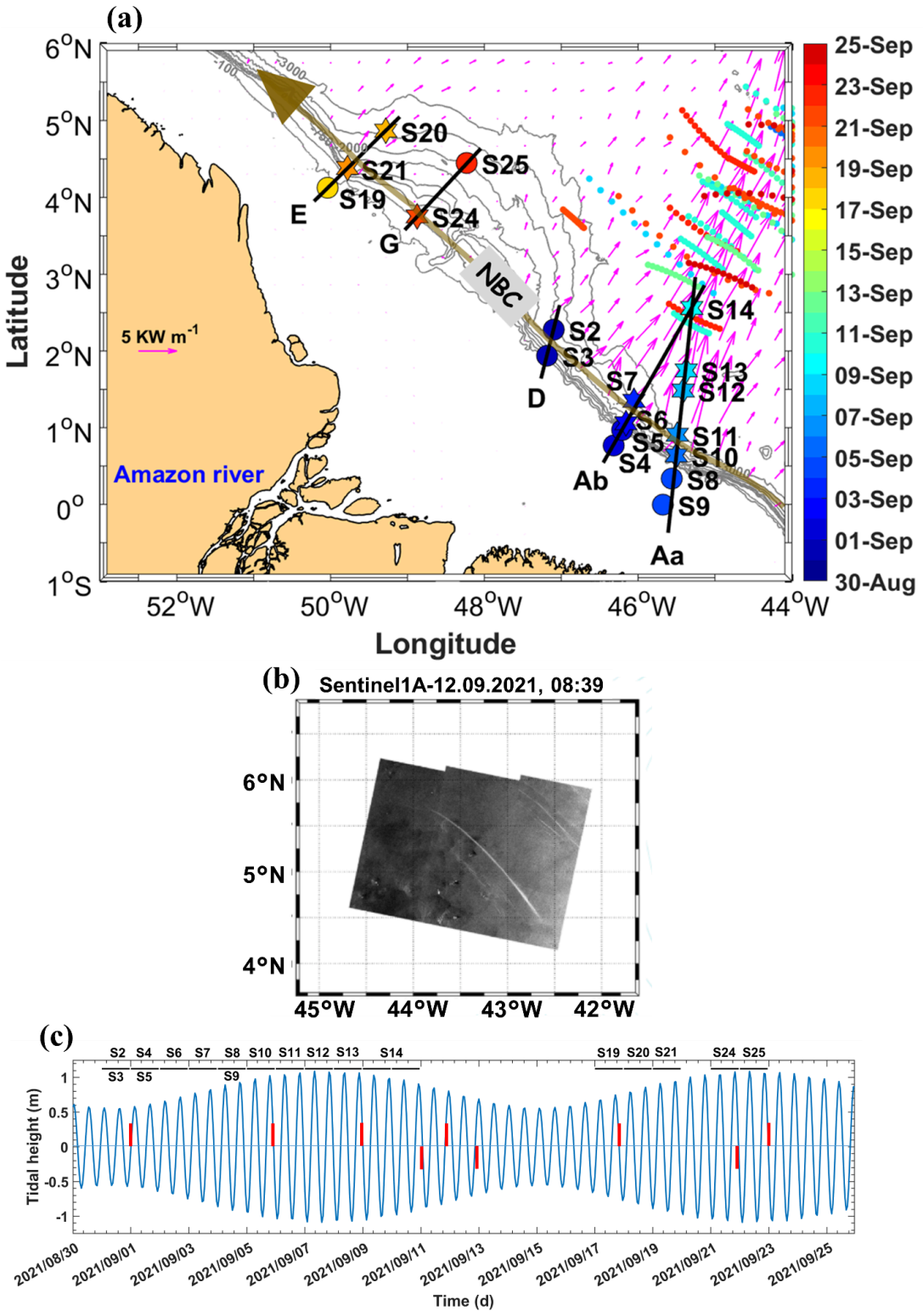

Figure 1: a) Map of a part of the AMAZOMIX 2021 cruise off the Amazon shelf, showing bathymetric contours (100 m, 750 m, 2000 m, and 3000 m isobaths) in gray. Colored circles and stars indicate short and long CTD-O2/L-S-ADCP stations, respectively, with the corresponding sampling dates represented by the color bar. Solid black lines depict SADCP transects (for Aa, Ab, D, G, and E). Magenta arrows show the 25-hour mean depth-integrated baroclinic IT energy flux (September 2015, from the NEMO model) originating from IT generation sites (Aa, Ab, D, and E) along the shelf break. The solid brown line represents the NBC pathways

illustrating background circulation. Shattered colored lines highlight ISW signatures. b) 1A Sentinel image acquired on 12th September 2021, showing ISW signatures. c) Tidal range at AMAZOMIX stations, with ISW signature dates marked by red bars.

“

-Baroclinic currents and energy : it is unclear why a parameterization of e is referred to as baroclinic total energy. The MG parameterization does not provide any relevant information (the correlation with epsilon is not clear and it is used as a proxy to evaluate the contribution of tidal shear and low frequency shear which I find questionable)

R: Thank you for your comment.

Indeed, the MacKinnon-Gregg parameterization was applied as a proxy to evaluate the contributions of tidal and low-frequency shear, primarily for comparison purposes. However, no scientific results were derived from it in this study.

Ultimately, we decided to remove the section using the parameterization and reserve the study and comparison of in-situ data to mixing parameterization for a separate paper in progress. In our paper, we used the vertical shear to assess the contributions of tidal and mean shear.

Revisions can be found in the "Methods" section, lines 122–235, as shown below:

“

2.2 Methods

TKE dissipation rates

The VMP data are processed using ODAS Matlab library (developed by Rockland Scientific International, Inc) to infer the TKE dissipation rate (ε). The processing methods for the VMP data are briefly described here and adhere to the recommendations of ATOMIX (Analyzing ocean turbulence observations to quantify mixing), as reported by Lueck et al. (2024), and have been validated against the benchmark estimates (presented in Fer et al., 2024).

First, the VMP data are converted into physical shear units, and the time series are prepared. Continuous sections of the time series are selected for dissipation estimation. Before spectral estimation, the aberrant shear signals caused by vessel wake contamination are removed. Collisions of the shear probe with plankton and other particles are removed using the de-spiking routine. The records from each section are then high-pass filtered (e.g., at station S6 and S10; Fig. 2a, and Fig. A1, Appendix).

Shear spectra are estimated using record lengths (L) and Fast Fourier Transform segments of 2 s, which are cosine windowed and overlapped by 50% (e.g., at station S6 and S10; Fig. 2b, and Fig. A1, Appendix). Additionally, vibration-coherent noise is removed. Different L and overlap (O) settings were selected and tested based on the environment (e.g., deep vs. shallow water), following Fer et al. (2024). For shallow stations, L (O) was shortened to 5 s (2.5 s), in contrast to the 8 s (4 s) used for deeper stations, due to evidence of overturns

observed in AMAZOMIX acoustic measurements at deeper stations (Koch-Larrouy et al., 2024; in preparation). This adjustment helped to optimize the spatial resolution of dissipation estimates in shallow water stations.

Finally, ε is determined using the spectral integration method and by comparison with the Nasmyth empirical spectrum (Nasmyth, 1970). Quality assurance tests are carried out in accordance with ATOMIX's recommendations (Lueck et al., 2024). A figure of merit < 1.4 is used to exclude bad data (e.g., at station S6 and S10; Fig. 2b, and Fig. A1, Appendix), and the fraction of data affected by de-spiking is < 0.05.

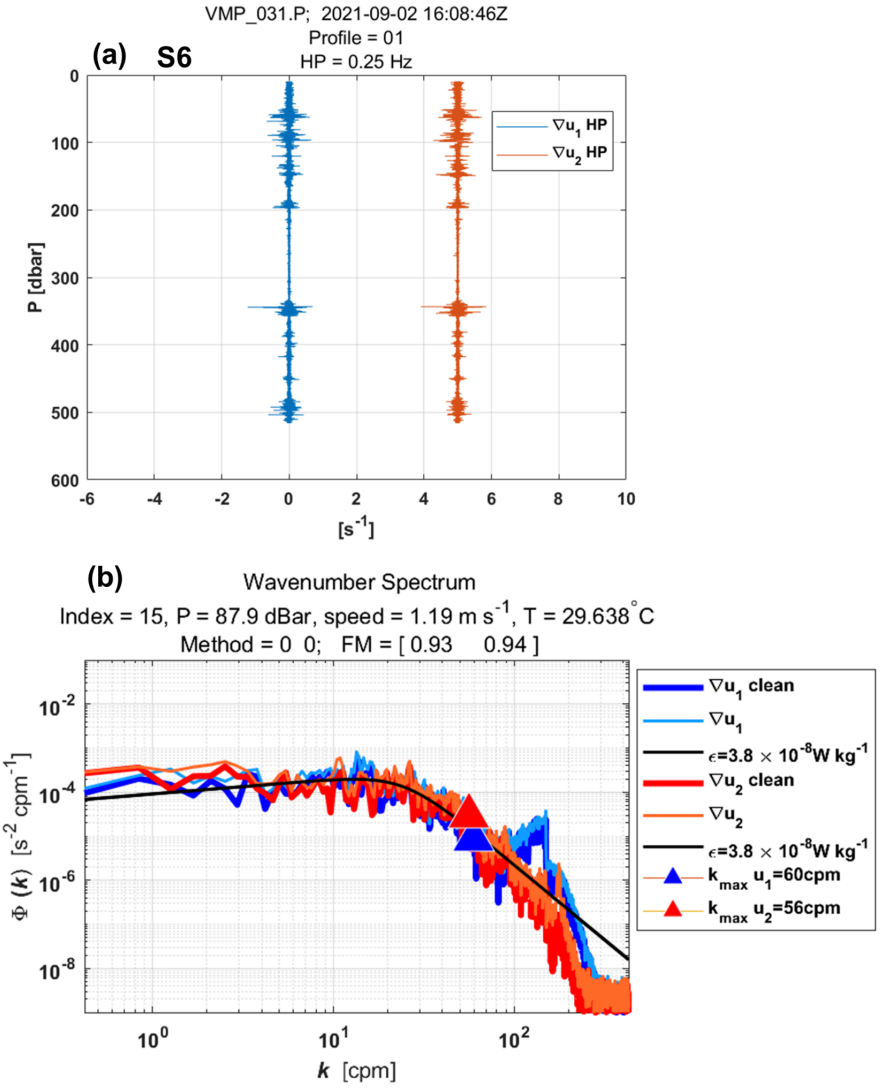

Figure 2: Example of wavenumber spectra from a dissipation structure segment used to determine the dissipation rate at station S6 at a pressure of 87.9 dBar. (a) Cleaned and high-pass filtered signals from shear probe 1 (blue) and shear probe 2 (red, offset by 5 s^{-1}). (b) Wavenumber spectra for shear probes 1 and 2. Thick lines (blue for probe 1, red for probe 2) show shear spectra with coherent noise correction, while thin lines (sky blue for probe 1, orange for probe 2) show spectra without correction. Triangles mark the maximum wavenumber used for dissipation rate estimation. Black lines represent Nasmyth reference spectra for estimated

dissipation rate of 3.8 x 10^{-8} W kg^{-1} for both shear probes. Dissipation rate estimates for shear probe 1 and shear probe 2 at a pressure of 87.9 dBar yielded a figure of merit of 0.93 and 0.94, respectively.

The vertical eddy diffusivity coefficient

The efficiency of turbulence in redistributing energy is assessed through the calculation of the vertical eddy diffusivity coefficient (K_z). This coefficient is particularly significant in regions such as pycnoclines, where stratification suppresses mixing, making turbulence-driven mixing a key mechanism for vertical energy transport (Thorpe, 2007).

K_z is calculated from ε following the formulation of Osborn (1980), given by $K_z = \varepsilon\ \Gamma\ N^{-2}$. Here, N^2 is the buoyancy frequency squared, which is calculated using the sorted potential density profiles (σ_θ) obtained from CTD-O_2 data. It is given by $N^2 = -\ (g/\rho_0)\ (d\sigma_\theta/dz)$, where ρ_0 is a reference density (1025 kg m^{-3}) and g is the gravitational acceleration. Γ is the mixing efficiency, defined as the ratio between the buoyancy flux and the energy dissipation, and is typically set to 0.2, which corresponds to the critical Richardson number Ri = 0.17 (Osborn, 1980). ε is linearly interpolated into the depths of N^2.

Turbulence within the pycnocline can reduce stratification and increase vertical eddy diffusivity below the mixing layer (Thorpe, 2007). Subsurface mixing, driven by the breaking of ITs and shear instabilities, plays a particularly important role below the mixed layer, especially in equatorial waters (Gregg et al., 2003).

There are several criteria for defining the Mixed Layer Depth (MLD). In this study, we use the commonly accepted density threshold criterion of 0.03 kg m^{-3}, as defined by de Boyer Montégut et al. (2004) and Sutherland et al. (2014), to estimate the MLD for each CTD-O_2 profile. Notably, comparisons with density thresholds of 0.01 and 0.02 kg m^{-3} revealed no major differences in MLD across the AMAZOMIX stations and transects (Fig. A2, Appendix).

The miXing Layer Depth (XLD) is defined as the depth at which ε decreases to a background level (Sutherland et al., 2014). Previous studies have applied various thresholds for background dissipation levels, such as such as 10^{-8} and 10^{-9} W kg^{-1} in higher latitudes based on in situ observations (Sutherland et al., 2014; Lozovatsky et al., 2006; Cisewski et al., 2008; Brainerd and Gregg, 1995) and 10^{-5} m^2 s^{-1} using an ocean general circulation model (Noh and Lee, 2008). In this study, XLD is specified as the depth where ε drops from its first minimum value. This aligns with previous dissipation thresholds and ensures that mixing is captured independently of surface influences. The Upper (UTD) and Lower (LTD/LPD) Thermocline/Pycnocline Depth are delimited as defined by Assunçao et al (2020). UTD corresponded to the depth where the vertical temperature gradient $\partial\theta/\partial z$ = 0.1 ℃ m^{-1}, while LTD/LPD were the last depth below the UTD at which $N^2 \geq 10^{-4}$ s^{-2}.

Baroclinic currents

To analyze the processes explaining dissipation and mixing, particularly along internal tidal (IT) paths, we estimate shear instabilities associated with the semi-diurnal (M2) ITs and mean circulation, as well as their contributions to mixing.

The M2 tidal component of the tidal current is derived by calculating the baroclinic (semi-diurnal) tidal velocity $[u'', v'']$ (Fig. A3, Appendix), following these equations:

$$[u', v'] = [u, v] - [u_{bt}, v_{bt}], \quad (1)$$

$$[u_{bt},\ v_{bt}] = \frac{1}{H}\int_{-H}^{0}[u,\ v]dz, \quad (2)$$

$$[u'',\ v''] = [u',\ v'] - [\overline{u'},\ \overline{v'}]. \quad (3)$$

Here, $[u,\ v]$ represent total horizontal velocities (Fig. A3, Appendix) obtained from SADCP data. The components $[u',\ v']$ and $[u_{bt},\ v_{bt}]$ represent baroclinic and barotropic components of horizontal velocities, respectively (Fig. A3, Appendix). H is water depth. The baroclinic mean velocities $[\overline{u'},\ \overline{v'}]$ (Fig. A3, Appendix), calculated to estimate mean circulation along IT paths, are decomposed into along-shore $\overline{u'}_l$ and cross-shore $\overline{u'}_c$ velocities. The overbar denotes the average over a M2 tidal period.

Note that continuously collected SADCP for some stations (e.g., S11) are not sufficiently resolved due to gaps filled by interpolating between time points. The similar processing are applied to the CTD-O_2 data collected alternately. SADCP time series data are less than 17 hours at all long stations, except for S14, which spans 42 hours. As a result, the diurnal and semidiurnal period fittings are not formally distinct (except at S14; Figs. A4 and A5, Appendix), and the inertial period (at least 5 days) cannot be resolved in our dataset. This limits our ability to separate currents by frequency and examine the associated dissipation.

The velocity profiles from LADCP are glued into our SADCP time series data below ~ 500 m depth at long stations.

To evaluate shear instabilities associated with ITs and the mean background circulation, we compute the baroclinic tidal vertical shear squared ($S^{2''}$) and mean shear squared ($\overline{S^{2'}}$) (Fig. A3, Appendix), as follows:

$$S^{2''} = (\partial u''/\partial z)^2 + (\partial v''/\partial z)^2, \quad (4)$$

$$\overline{S^{2'}} = (\partial \overline{u'}/\partial z)^2 + (\partial \overline{v'}/\partial z)^2. \quad (5)$$

To evaluate the impact of bottom friction on mixing, we calculate kinetic energy $\varepsilon_f = \frac{1}{2}\rho_s(u_f^2)$ near the bottom boundary layer at shallow stations using friction velocity $u_f = u_b\sqrt{C_d}$, where C_d=2.5 x 10^{-3} is a drag coefficient obtained from the NEMO model. Huang et al. (2019) showed that the bottom boundary layer thickness spatially varies between 15-123 m in the Atlantic Ocean, with a median of ~ 30-40 m in the North Atlantic. We define bottom layer thicknesses in our study area based on measured bathymetry from CTD-O_2 and near-bottom currents from ADCP. Here, u_b is the total velocity averaged over a thickness of 20 m above the seabed for shallow stations and 40 m for deep stations.

The individual contributions of semi-diurnal ITs and mean circulation are then expressed as follows: $E''/(\overline{E'} + E'')$ for tidal contribution and $\overline{E'}/(\overline{E'} + E'')$ for mean circulation contribution. Here, $E = N^2S^2$. N is the buoyancy frequency and S is vertical shear. S can be substituted by $S^{2''}$ and $\overline{S^{2'}}$.

Ray tracing calculation

Analyzing both the mean currents and the spatial dimension along the IT pathways offers another insight into the mechanisms responsible for observed mixing (Rainville and Pinkel, 2006). IT energy rays are generated in

regions with steep topography, such as the shelf break, where IT slope matches with the bottom slope (i.e., critical slopes) before propagating within the ocean interior. These rays, moving both downward and upward, encounter the seasonal pycnocline, resulting in beam scattering and the formation of large IT oscillations. As these oscillations steepen, they disintegrate into nonlinear ISWs, a process known as "local generation" of ISWs (New and Pingree, 1992). To explore IT paths, ray-tracing techniques are employed, as previously used by New and Da Silva (2002) and Muacho et al. (2014), to investigate the effectiveness and expected pathways of the IT beams off the Amazon shelf. One main assumption in our linear-theory-based hypothesis is that stratification remains horizontally uniform along the IT propagation path, although in reality, it may vary due to submesoscale and mesoscale variability. This limitation makes the ray tracing approach less realistic but still useful as a first-order estimate of energy distribution. The IT ray-tracing calculation assumes that in a continuously stratified fluid, ITs energy can be described by characteristic pathways of beams (or rays) with a slope c to the horizontal:

$$c = \pm\left(\frac{\sigma^2 - f^2}{N^2 - \sigma^2}\right)^{1/2}, \qquad (6)$$

where σ is the M2 tidal frequency (1.4052×10^{-4} rad s^{-1}), and f is the Coriolis parameter. N^2 are obtained from time-averaged AMAZOMIX CTD-O_2, glued with monthly N^2 profiles from Amazon36 (NEMO model outputs, 2012-2016) below 1000 m depth. Amazon36 is a NEMO configuration, specifically designed to cover the western tropical Atlantic from the mouth of the Amazon River to the open sea (see Tchilibou et al., 2022; Assene et al., 2024; for configuration details and model description). IT ray-tracing diagrams are performed along the transects. Seasonal sensitivity tests of rays (August, September, October, and April) are conducted by varying the critical slope positions and N^2 to explore its influence and generate a set of ray paths consistent with characteristics of IT pathways (Figs. A6 and A7, Appendix).

”

-Ray tracing calculation is applied but horizontal density gradients are neglected : this assumption is surprising owing to the major influence of the mean baroclinic flow.

Also in Figure 5 it would be more clear regarding the IT ray paths to consider the full water column

R: Thank you for your comment.

Indeed, our ray-tracing calculation neglected horizontal density gradients and the mean baroclinic flow, which we acknowledge as a limitation. In our study, the ray-tracing calculation superimposed with mean current data is used as another tool to gain insights into the mechanisms driving the observed mixing along the IT path. Indeed, change in density along the propagation path will affect the wavelength and beams of the rays.

To try to assess the potential influence of horizontal density gradients, we have tested different N2 profiles at specific stations (e.g., S10, S12, and S14) along transect Aa. The sensitivity tests (Figure RC2.1) demonstrated that ray paths align within the packets of rays observed when using mean N2 profiles at different times (e.g., in September and October; Figure RC2.2). Similarly, the influence of mean circulation could be very important for the ray. This question is beyond the scope of this study, and is tackled in

another paper we are working on using model results. Both influences-stratification and background circulation—are discussed in the sections "Methods" (lines 233–235) and "Results" (lines 401–423) of the revised manuscript.

In Figure 5 of the revised manuscript, we considered the full water column for internal tide (IT) ray paths, as depicted in the figure RC2.2. However, the y-axis in the manuscript is limited to 1000 m depth to enhance the visibility of dissipation profiles, density/stratification.

The influence of stratification and mean current on mixing and IT ray paths using ray-tracing calculations will be explored in a separate modelling paper.

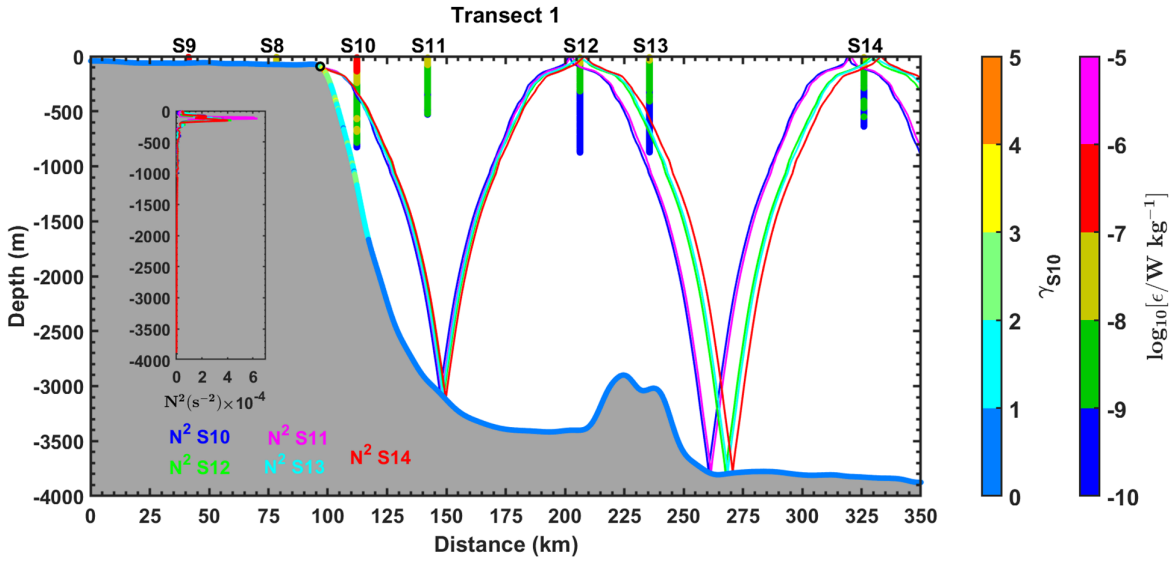

figure RC2.1: Example of sensitivity tests with different cross-sectional measurements of N^2 along the transect T1 N^2. colors are used to distinguish different cross-shore measurements of N^2 for corresponding stations on T1. Topography steepness (gamma = ray slope / topography slope) for T1 using measured N^2 of S10. Gamma is illustrated by the colored bar (named gamma S10).

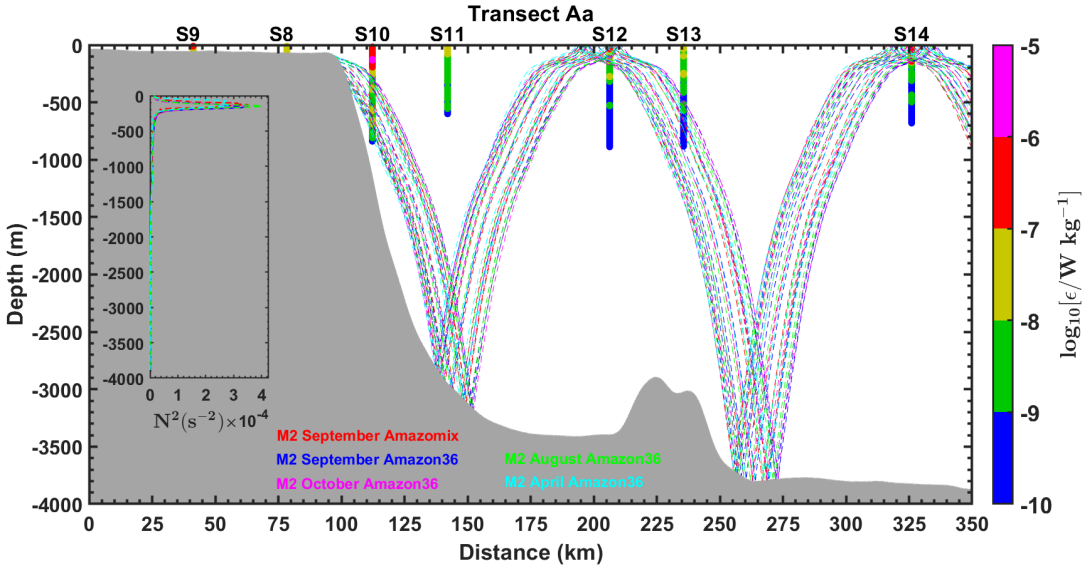

figure RC2.2: Sensitivity tests of M2 IT ray-tracing along the transects Aa, conducted by varying the location of the critical topography slope. The tests use mean buoyancy frequency squared (N^2, in s^{-2}) obtained from CTD-O_2 data (September 2021) and NEMO-Amazon36 model data (2012-2016). Dashed colored lines represent IT beams calculated for different seasons (April, August, October, and September) and for varying locations of the critical topography slope. Grey areas indicate local topography. Panel also includes dissipation rate profiles (ε, in W kg^{-1}, shown as vertical colored bars on a logarithmic scale) from the VMP measurements. Subpanels within each panel illustrate the N^2 profiles derived from AMAZOMIX and the NEMO-Amazon36 model, which were used in the ray-tracing calculations. For comparison, sensitivity tests using N^2 measurements from individual stations along the corresponding transect (e.g., at S10) revealed similar ray paths (not shown), consistent with the packet of rays obtained using the mean N^2.

Revisions can be found in the "Methos/Ray tracing calculation" section, in lines 223–226 and 233-235 of revised manuscript, as shown below:

“

One main assumption in our linear-theory-based hypothesis is that stratification remains horizontally uniform along the IT propagation path, although in reality, it may vary due to submesoscale and mesoscale variability. This limitation makes the ray tracing approach less realistic but still useful as a first-order estimate of energy distribution..

“

“

Seasonal sensitivity tests of rays (August, September, October, and April) are conducted by varying the critical slope positions and N^2 to explore its influence and generate a set of ray paths consistent with characteristics of IT pathways (Figs. A6 and A7, Appendix)..

“

-Figure 3 : it is difficult to have a view on the evolution along the transects, why not show e profils along the transect with density superimposed, some large values at the end of the e profils would need to be checked (S12 and S14 in Fig. 3. and 3.e as well as S2 figA.1.c)

R: Thank you for your comment.

Indeed, the evolution of dissipation profiles, as well as, density along the transect were shown in Figure 8 of revised manuscript and figures in appendix. An example is shown in the figure RC2.4 below.

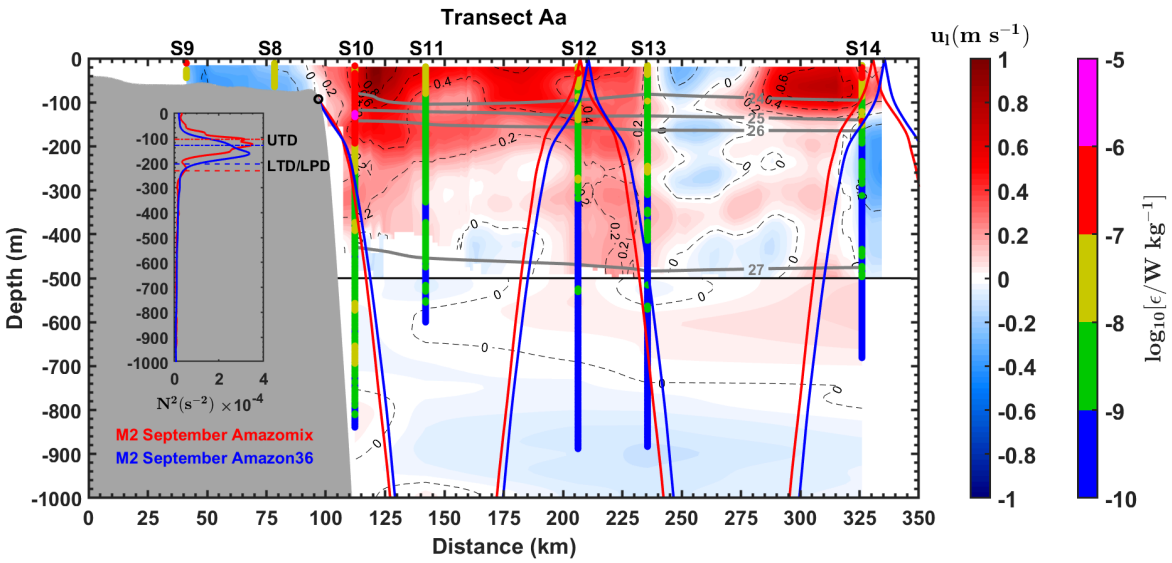

Figure RC2.4: IT ray-tracing diagrams for the M2 tidal constituent along transects Aa. The calculations were performed using the mean buoyancy frequency squared (N^2, in s^{-2}) obtained from CTD-O_2 data (ray in red) and NEMO-Amazon36 model data (ray in blue) for September. Grey areas represent local topography and black circles indicate the critical topography slope (ray generation sites). Panel also show along the transects Aa: along-shore mean total currents (u_l, in m s^{-1}) from ADCP (Dashed black lines), potential density from CTD-O_2 (grey contours), and dissipation rate profiles (ε, in W kg^{-1}, on a logarithmic scale) from the VMP (vertical colored bars). Subpanels within each panel illustrate the N^2 profiles from AMAZOMIX (red line) and the NEMO-Amazon36 model (blue line) used for ray-tracing calculations. Upper Thermocline Depth (UTD, dotted lines) and Lower Thermocline/Pycnocline Depth (LTD/LPD, dashed lines) are also indicated.

We have revised the important values at the end of the e profiles at these stations (S12, S14, and S2).

Revisions and checks of the VMP profile processing and dissipation estimates have been carried out, along with quality assurance tests, in alignment with all reviewers' comments and ATOMIX's recommendations (Lueck et al., 2024).

a) First, the revisions were focused on the VMP profile processing, particularly on:

- Parameters controlling shear spectra estimation, such as record lengths (L), which are cosine-windowed and overlapped (O) by 50%.
- Parameter for extracting the section or profile (continuous part of the time series), including the minimum depth of extraction (Pmin).

For shallow stations, we used L = 5 s and O = 2.5 s, instead of the previous L = 4 s and O = 2 s. Parameters for deep stations remain unchanged (L = 8 s and O = 4 s).

Additionally, we adjusted the minimum depth of extraction to Pmin = 10 m for deep stations and Pmin = 3 m for shallow stations, compared to the previously used value of Pmin = 1 m for both station types.

b) Second, the revisions and checks focused on the quality assurance measures for dissipation estimates, with quality control checks and adjustments applied across all stations (e.g., S2, S7, S12, S14).

For instance, at station S14, previous dissipation estimates showed some peaks at various depths, particularly between 100–200 m, 300–400 m, and 500–700 m. While the fraction of shear data affected by despiking during processing was <0.05, the figure of merit (FM)—used to filter out poor-quality data—for shear probe 1 was >>1.4 at certain depths (e.g., around 327 m compared to 122 m, as shown in figure RC2.5). In contrast, the FM for shear probe 2 remained <1.4.

After checks, quality control of dissipation estimates have been revised for all stations (e.g., S6, S10, S14). We have retained only dissipation estimates from either one or both probes that met the quality assurance criteria (FM < 1.4 and fraction of despiked shear data <0.05, as recommended by ATOMIX), as shown at S6 and S10 for example (figure RC2.6).

The final dissipation estimate was computed as the average of the estimates from both shear probes, followed by the mean of the dissipation profiles for the station, as illustrated in figure RC2.7.

The revision of section “methods/TKE dissipation rates” can be found in lines 169-194, in text, as shown below:

“

The VMP data are processed using ODAS Matlab library (developed by Rockland Scientific International, Inc) to infer the TKE dissipation rate (ε). The processing methods for the VMP data are briefly described here and adhere to the recommendations of ATOMIX (Analyzing ocean turbulence observations to quantify mixing), as reported by Lueck et al. (2024), and have been validated against the benchmark estimates (presented in Fer et al., 2024).

First, the VMP data are converted into physical shear units, and the time series are prepared. Continuous sections of the time series are selected for dissipation estimation. Before spectral estimation, the aberrant shear signals caused by vessel wake contamination are removed. Collisions of the shear probe with plankton and other particles are removed using the de-spiking routine. The records from each section are then high-pass filtered (e.g., at station S6 and S10; Fig. 2a, and Fig. A1, Appendix).

Shear spectra are estimated using record lengths (L) and Fast Fourier Transform segments of 2 s, which are cosine windowed and overlapped by 50% (e.g., at station S6; Fig. 2b, and Fig. A1, Appendix). Additionally, vibration- coherent noise is removed. Different L and overlap (O) settings were selected and tested based on the environment (e.g., deep vs. shallow water), following Fer et al. (2024). For shallow stations, L (O) was shortened to 54s (2.5s), in contrast to 8 s (4 s) used for deeper stations, due to evidence of overturns observed in AMAZOMIX acoustic measurements at deeper stations (Koch-Larrouy et al.,

2024; in preparation). This adjustment helped to optimize the spatial resolution of dissipation estimates in shallow water stations.

Finally, ε is determined using the spectral integration method and by comparison with the Nasmyth empirical spectrum (Nasmyth, 1970). Quality assurance tests are carried out in accordance with ATOMIX's recommendations (Lueck et al., 2024). A figure of merit < 1.4 is used to exclude bad data (e.g., at station S6; Fig. 2b, and Fig. A1, Appendix), and the fraction of data affected by de-spiking is < 0.05.

”

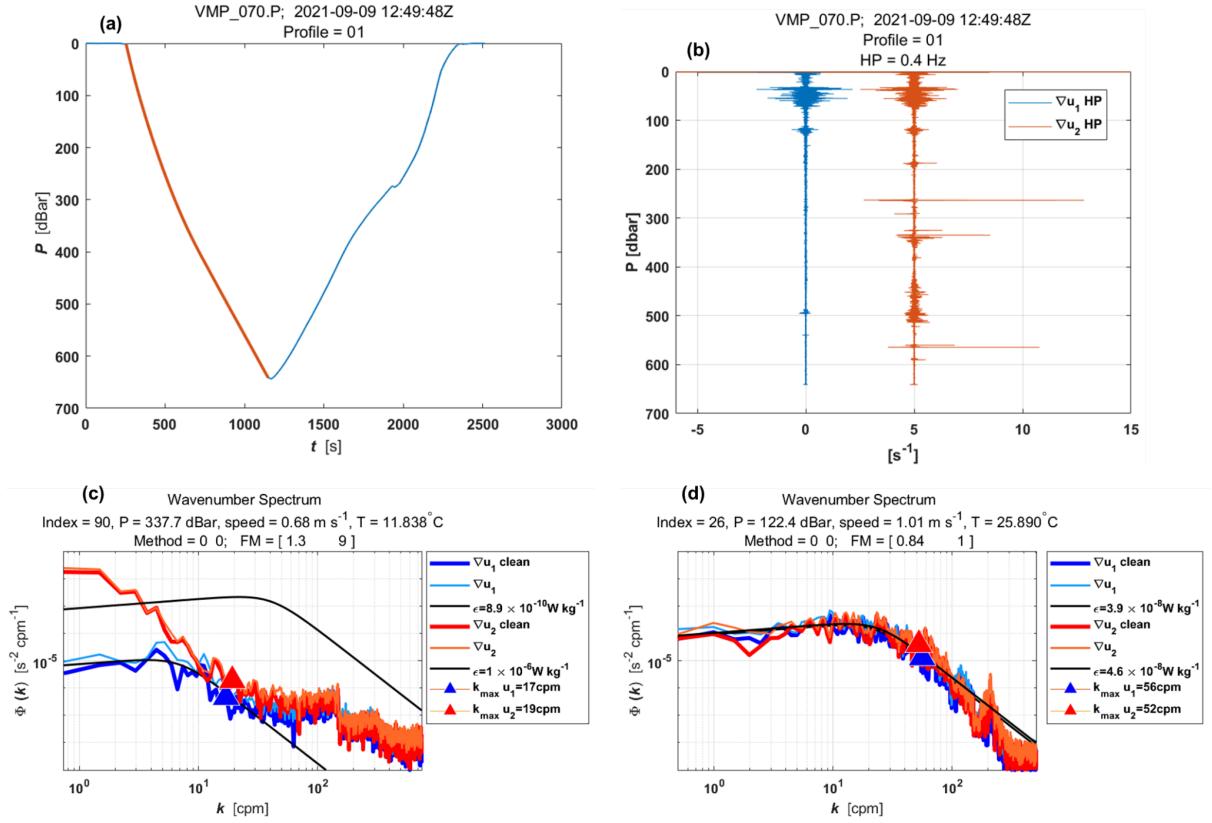

Figure RC2.5: Example of wavenumber spectra from a dissipation structure segment used to determine the dissipation rate at station S14 at a pressure of 337.7 dBar. (a) Pressure record for the entire data file (blue) and the specific segment being analyzed (red). (b) Cleaned and high-pass filtered signals from shear probe 1 (blue) and shear probe 2 (red, offset by 5 s^{-1}). (c) Wavenumber spectra for shear probes 1 and 2. Thick lines (blue for probe 1, red for probe 2) show shear spectra with coherent noise correction, while thin lines (sky blue for probe 1, orange for probe 2) show spectra without correction. Triangles mark the maximum wavenumber used for dissipation rate estimation. Black lines represent Nasmyth reference spectra for estimated dissipation rate of 8.9 x 10^{-10} W kg^{-1} and 1 x 10^{-6} W kg^{-1} for shear probes 1 and 2, respectively. Dissipation rate estimates for shear probes 1 and shear probe 2 at a pressure of 337.7 dBar yielded a figure of merit of 1.3 and 9, respectively. Panel (d) is similar to panel (c) but:- with Nasmyth reference spectra for estimated dissipation rate of 3.9 x 10^{-8} W kg^{-1} and 4.6 x 10^{-8} W kg^{-1} for shear probes 1 and 2. -wth dissipation rate estimates for shear probes 1 and 2 at a pressure of 122.4 dBar yielding a figure of merit of 0.84 and 1, respectively.

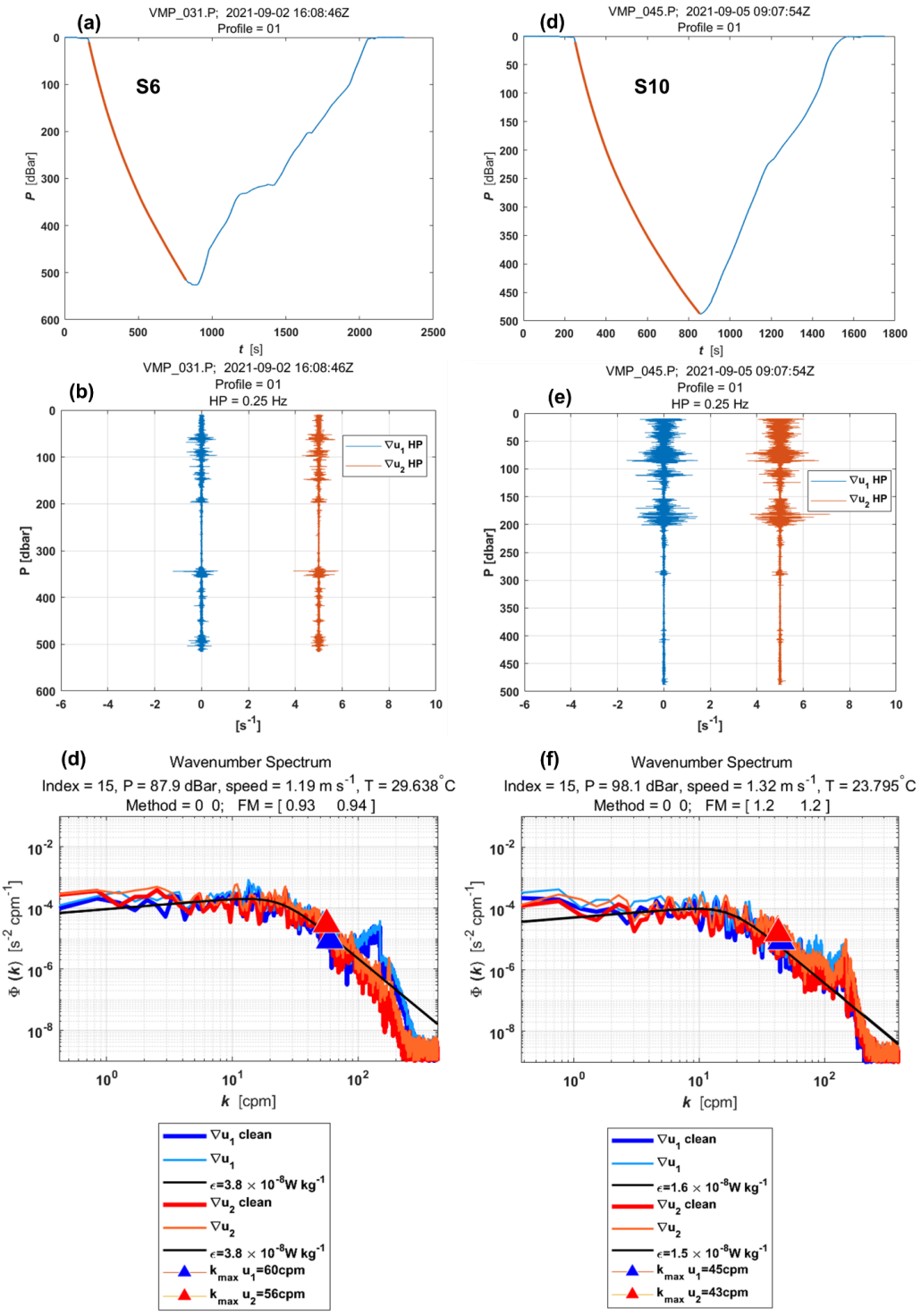

Figure RC2.6: Similar to Fig. RC1.1. but for stations (a)-(b)-(c) S6 and (d)-(e)-(f) S10. For S6 (panels c), Black lines represent Nasmyth reference spectra for estimated dissipation rate of 3.8 x 10-8 W kg-1 for both shear probes, and dissipation rate estimates for shear probes 1 and shear probe 2 at a pressure of 337.7 dBar yielded a figure of merit of 0.93 and 0.94, respectively. For S10 (panel f), Black lines represent Nasmyth reference spectra for estimated dissipation rate of 1.6 x 10^{-8} W kg^{-1} and 1.5 x 10^{-8} W kg^{-1} for shear probes 1 and 2, respectively, and dissipation rate estimates for both shear probes at a pressure of 337.7 dBar yielded a figure of merit of 1.2.

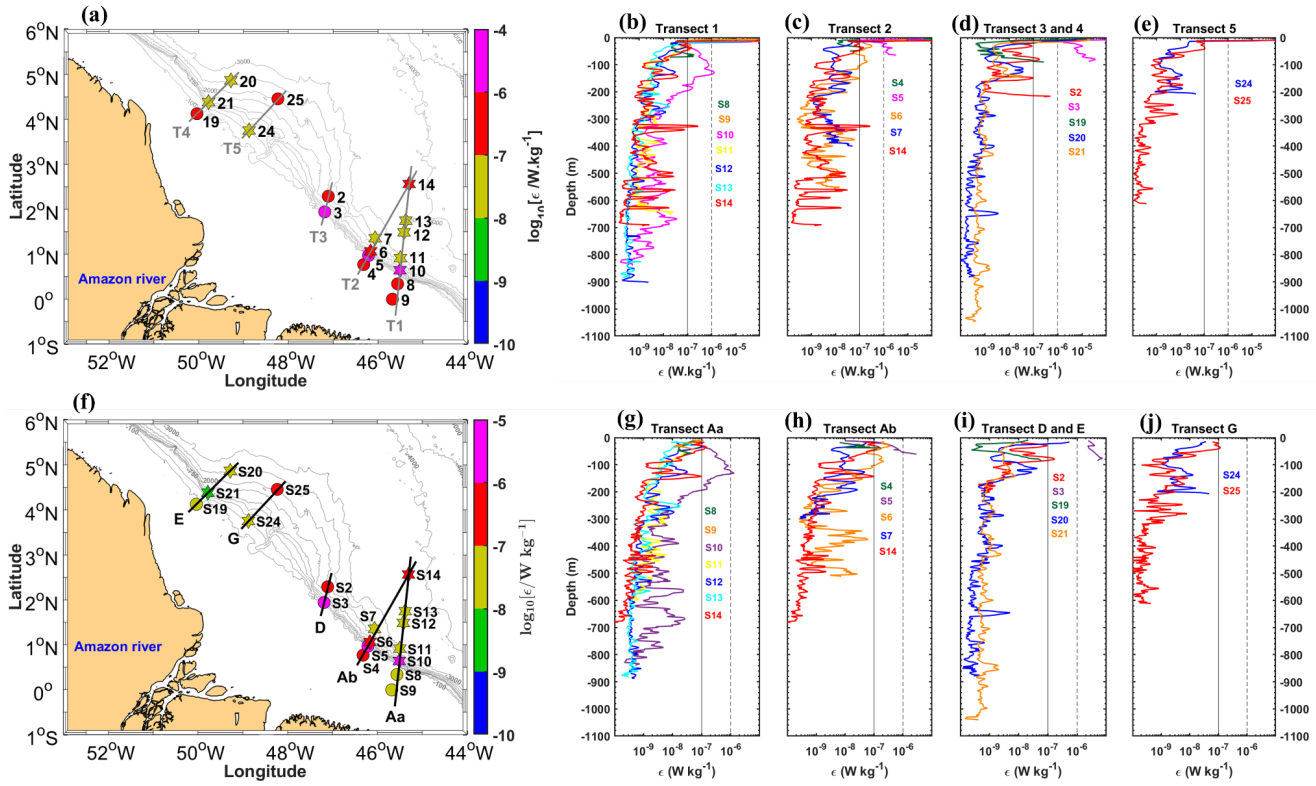

figure RC2.7: (a) Horizontal maximum and (b)-(c)-(d)-(e) vertical dissipation rates (ε, in W kg-1, on a logarithmic scale) before revisions and checks processes for all stations along transects T1 to T2. (f) Horizontal maximum and (g)-(h)-(i)-(j) vertical dissipation rates (ε, in W kg-1, on a logarithmic scale) after revisions and checks processes for all stations along transects Aa, Ab, D, E, and G. Distinct colors are used to represent each station within each transect. Dashed and solid black lines in panels (b) to (e) are included for comparison purposes.

-the relationship between step-like structures and strong internal tides is not convincing as it is presented

R: We agree that without prior knowledge of step-like features, this action can be difficult to understand. Thank you for highlighting this. In response, we have added arrows in Figure 3 of manuscript to indicate the "step-like structures" and "vertical displacement," making it easier for readers to understand the "step-like features" we are referring to (see figure RC2.8 below).

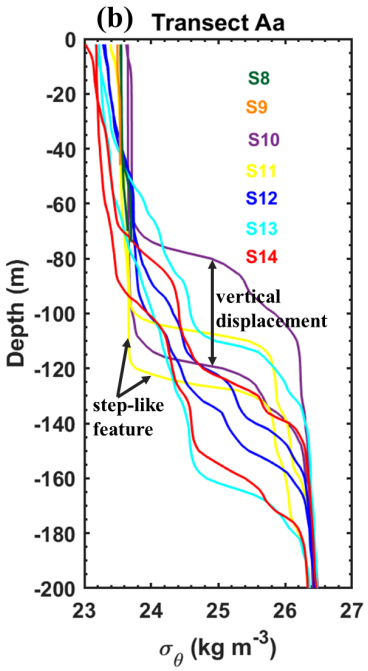

figure RC2.8: *Density profiles (σ_θ, kg m^{-3}) obtained from CTD-O_2 measurements during the AMAZOMIX 2021 cruise for stations S8 to S14 along transects Aa, located within IT fields. For long stations (S10-S14), two density profiles are shown to highlight step-like structures and isopycnal vertical displacements (illustrated by black arrows) along the transects. Distinct colors are used to represent each station within transect. The density values for stations S8, and S9 range between 23.4 and 23.8 kg m^{-3}*

-Figure 4 : Emphasis is made on shear instability, this is quite convincing at S10 but not at S14, this should be interesting to comment on.

R: Thank you for your comment.

Indeed, the focus is on the contribution of tidal and low-frequency shear instability in the mixing process. It was found that tidal shear and its influence are stronger at S10, located near the tidal generation site, compared to S14, which is farther from the generation site in the open ocean. This is discussed in the section "Discussion and Conclusion" (lines 435–569), with particular emphasis at S14 in lines 551–566 of the revised manuscript, as shown below at the end of this document.

-Competitive processes to generate mixing: the hypothesis of shear-driven dissipation is followed with the aim to discriminate between the low frequency shear contribution and the IT shear one. I find this subsection difficult to follow, and I don't understand why the MG parameterization is introduced to this aim.

R: Thank you for your comment.

Indeed, the MacKinnon-Gregg parameterization was applied as a proxy to evaluate the contributions of tidal and low-frequency shear, primarily for comparison purposes. However, no scientific results were derived from it in this study.

Ultimately, we decided to remove and reserve the mixing parameterization for a separate paper in progress. Instead, we revised the subsection and focused on vertical shear to assess the contributions of tidal and mean shear.

-Figure 5 : the ray tracing approach should be revisited with taking into account the low frequency current, mean along shore current displays some spatial variations that may modify the ray structure ;

R: Thanks for your comment.

Indeed, our ray-tracing calculation neglected horizontal density gradients and the mean baroclinic flow, which we acknowledge as a limitation. In our study, the ray-tracing calculation superimposed with mean current data is used as another tool to gain insights into the mechanisms driving the observed mixing along the IT path.

To try to assess the potential influence of horizontal density gradients, we tested N2 profiles at specific stations (e.g., S10, S12, and S14) along transect Aa. The sensitivity tests (Figure RC2.9) showed that ray paths align within the packets of rays observed when using mean N2 profiles at different times (e.g., in September and October; Figure RC2.10). Similarly, the influence of mean circulation was evaluated by superimposing on the figure RC2.10 the mean total current, as shown in the corresponding figure 8 of manuscript revised.

Both influences—stratification and background circulation—are discussed in the sections "Methods" (lines 233–235) and "Results" (lines 401–423) of the revised manuscript.

The influence of stratification and mean current on mixing and IT ray paths using ray-tracing calculations will be explored more in a separate paper.

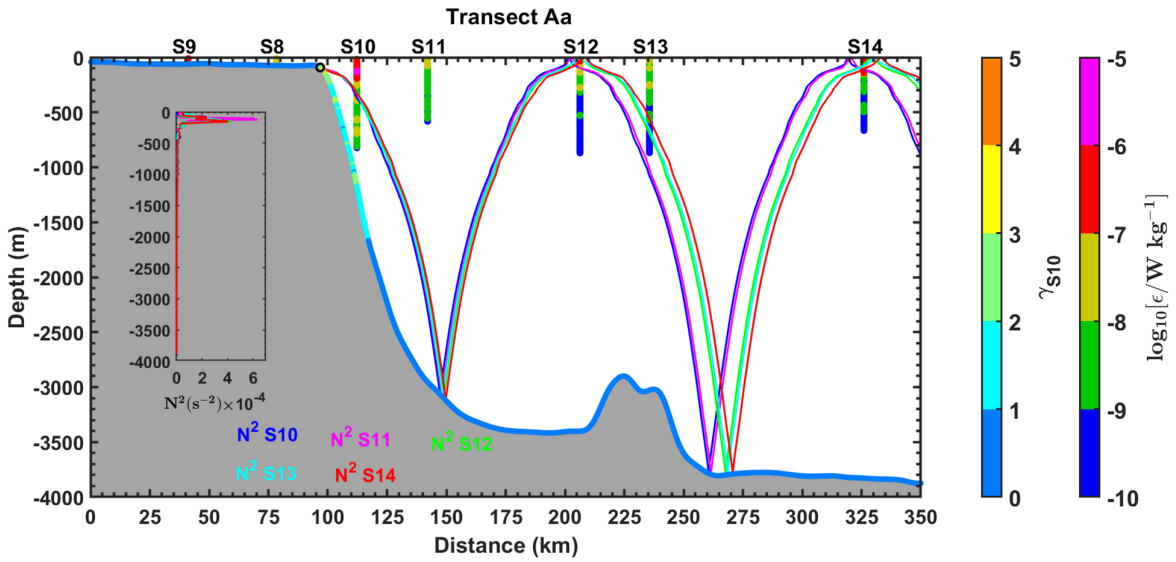

figure RC2.9: Example of sensitivity tests with different cross-sectional measurements of N^2 along the transect T1 N^2. colors are used to distinguish different cross-shore measurements of N^2

for corresponding stations on T1. Topography steepness (gamma = ray slope / topography slope) for T1 using measured N^2 of S10. Gamma is illustrated by the colored bar (named gamma S10).

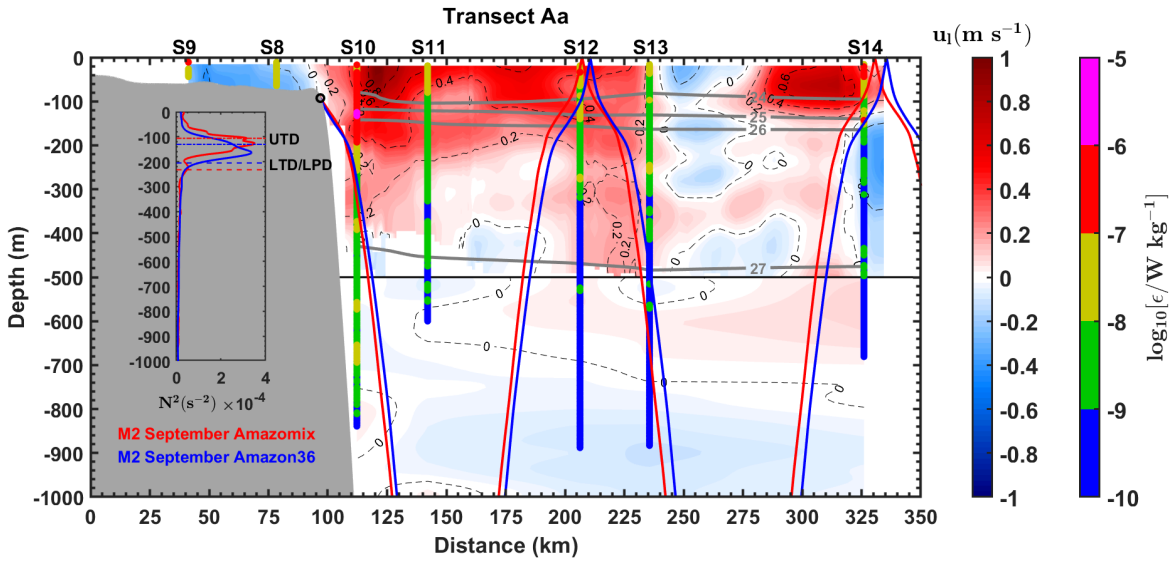

figure 10: IT ray-tracing diagrams for the M2 tidal constituent along transects Aa. The calculations were performed using the mean buoyancy frequency squared (N^2, in s^{-2}) obtained from CTD-O_2 data (ray in red) and NEMO-Amazon36 model data (ray in blue) for September. Grey areas represent local topography and black circles indicate the critical topography slope (ray generation sites). Panel also show along the transects Aa: along-shore mean total currents (u_l, in m s^{-1}) from ADCP (Dashed black lines), potential density from CTD-O_2 (grey contours), and dissipation rate profiles (ε, in W kg^{-1}, on a logarithmic scale) from the VMP (vertical colored bars). Subpanels within each panel illustrate the N^2 profiles from AMAZOMIX (red line) and the NEMO-Amazon36 model (blue line) used for ray-tracing calculations. Upper Thermocline Depth (UTD, dotted lines) and Lower Thermocline/Pycnocline Depth (LTD/LPD, dashed lines) are also indicated.

-Nutrients fluxes : profiles of Kz and nutrients fluxes are displayed. I don't see the point in giving values of nutrients fluxes without showing the concentration profiles and introduce the motivations and the issues.

R: Thanks for your comment.

Indeed, nutrient concentration profiles were analyzed prior to calculating nutrient fluxes.

Ultimately, we decided to remove and reserve all sections on “Nutrients fluxes” for a separate paper in progress.

-Discussion and conclusion : needs to be re-written and with convincing results for most part of it, one example : l442 « shear instabilities stronger >10-4s-2 », IT shear : high tidal modes are referred to but not shown etc

R: Thanks for your comment.

We have revised and rewritten the "Discussion and Conclusion" section, with updates found between lines 551–569 of the revised manuscript.
The tidal modes identified in the baroclinic tidal current time series (see figure RC2.11 below for an example) are presented in the section "Results" of the revised manuscript.

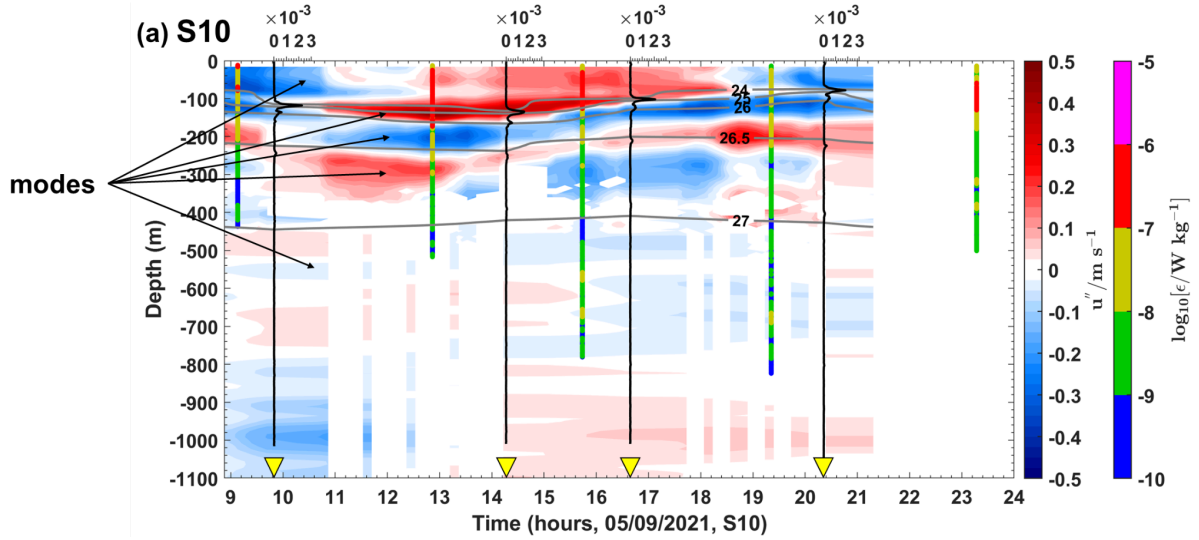

figure 11: Semi-diurnal baroclinic zonal currents (u", in m s-1) from the ADCP for stations (a) S10. Panel (a) also displays the buoyancy frequency squared (N2, in s-2) represented by vertical black lines, potential density represented by grey contours, and dissipation rate profiles (ε, in W kg-1, on a logarithmic scale) represented by vertical colored bars.

Revisions of section “Discussion and Conclusion” can be found below:

.

“

4 Discussion and Conclusion

The AMAZOMIX 2021 cruise provided, to the best of our knowledge, for the first time, direct measurements of turbulent dissipation using a velocity microstructure profiler (VMP) at multiple stations both inside and outside the influence of ITs. These measurements enabled the study of mixing processes at the Amazon Shelf break and the adjacent open ocean. To capture a full tidal cycle, data on turbulent dissipation rates, hydrography, and currents were collected alternately over 12 hours, with 4 to 5 profiles taken per station (see section 2). The locations of the 12-hour sampling stations were selected based on modeling results that provided realistic maps of IT generation and propagation (Fig. 1a; Tchilibou et al., 2022). Stations were located in the most energetic regions of IT, specifically at sites Aa, Ab, and D, covering stations S2 to S14, as identified in previous studies (Magalhaes et al., 2016; Tchilibou et al., 2022; Assene et al., 2024). Stations S19 to S21 were positioned in less energetic IT generation areas at site E, while stations S24 and S25 were located outside the influence of the IT fields (site G). Stations were distributed across different areas, including the shelf (e.g., S4, S9, and S19), the shelf-break (e.g., S3, S6, and S10), and the open ocean (e.g., S14, S24, and S20).

Vertical Displacement, homogeneous layers

The results revealed that, over a semi-diurnal tidal cycle, relevant amplitudes of vertical displacements (up to 60 m in length) and pronounced step-like structures (up to 40 m thick) were observed along transects Aa and Ab. In contrast, smaller and thinner structures were identified along other transects, such as E. These differences are likely related to the propagation of ITs, which induce vertical displacements at tidal frequencies and promote mixing by creating homogeneous layers visible as step-like features in the density structure. The isopycnal displacements and step-like structures observed within the pycnocline are consistent with findings from other IT regions (e.g., Stansfield et al., 2001; Simpson and Sharples, 2012; Bordois, 2015; Koch-Larrouy et al., 2015; Zhao et al., 2016; Bouruet-Aubertot et al., 2018; Xu et al., 2020). Furthermore, IT propagation appears to have stronger energy along transects Aa and Ab compared to others, consistent with prior modeling studies (Tchilibou et al., 2022; Assene et al., 2024).

Direct measurements of dissipation rate

Dissipation rates measured with the VMP ranged from between [10^{-10}, 10^{-5}] W kg^{-1} below the XLD, spanning from the continental shelf to the open ocean. The XLD was found to be considerably larger than the MLD at all stations, except at S8, S10, and S25. This is consistent with regions exhibiting strong subsurface shear, such as the equatorial ocean and western boundary current areas (Noh and Lee, 2008). The exception observed at other stations may reflect larger mixing events that were not captured by the VMP measurements.

The highest dissipation rates, within [10^{-6}, 10^{-5}] W kg^{-1}, were observed primarily at generation sites Aa, Ab, and D (e.g., at stations S6, S10, and S3). Slightly lower but still substantial dissipation rates, ranging from 10^{-8} to 10^{-7} W kg^{-1}, occurred a few kilometers (~40 km) from these generation sites (e.g., at S11 and S7), along IT pathways (e.g., at S12, S13, and S20), and even in regions farther from IT influence (e.g., at S24). Interestingly, dissipation rates were higher within [10^{-7}, 10^{-6}] W kg^{-1} in the open ocean, such as at station S14, located ~230 km from generation site Aa, as summarized in Fig. 9.

Similarly, the vertical eddy diffusivity coefficient, ranging from 10^{-3} to 10^{-1} m^2 s^{-1}, was highest at the shelf-break (at stations S3, S5, and S10), Away from the shelf-break, diffusivity values were lower but still substantial, within [10^{-4}, 10^{-3}] m^2 s^{-1} (e.g., at S2, S7, and S11).

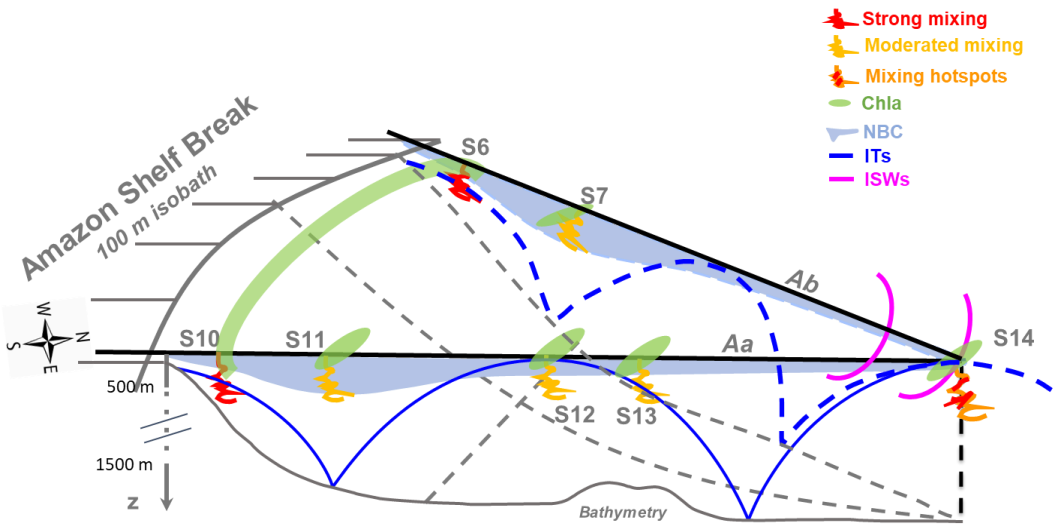

Figure 9: summary diagram illustrating the key processes driving mixing along the AMAZOMIX transects (e.g., Aa and Ab). At IT generation sites (e.g., S6 and S10), mixing rates are stronger, with ITs contributing around 65%, compared to mean circulation (NBC). Along IT pathways (e.g., S7 and S11), mixing decreases but remains notable, driven by nearly equal contributions from ITs and mean circulation. A key observation is the increased mixing ~ 230 km from two distinct IT generation sites at the shelf break. This hotspot at S14 coincides with the surfacing of IT rays from different sites and the presence of ISWs, suggesting that constructive interference of IT rays may generate ISWs, amplifying mixing at S14.

In comparison, in other regions, dissipation rates measured by similar VMP instrument are found between [10^{-7}, 10^{-5}] W kg^{-1} in the IT generation zone of Halmahera Sea, Indonesia (Koch-Larrouy et al., 2015; Bouruet-Aubertot et al., 2018), of Kaena Ridge, Hawaii (Klymak et al., 2008) and off the Changjiang Estuary (Yang et al. 2020). Whereas it is [10^{-10},10^{-8}] W.kg^{-1} along the IT path in the Southern Ocean (Gille et al., 2012) and in Halmahera Sea (Bouruet-Aubertot et al., 2018). Direct estimates of dissipation are almost [10^{-11}, 10^{-10}] W kg^{-1} far from IT influence (Koch-Larrouy et al., 2015; Bouruet-Aubertot et al., 2018) or under the influence of geostrophic current (Takahashi and Hibiya, 2019).

Our mixing coefficients are consistent with, the annual mean between [10^{-4}, 10^{-3}] m^2 s^{-1} of Ffield and Gordon (1992) or Koch-Larrouy et al. (2007), and aligned with others previous studies using the microstructure data (e.g. Tian et al., 2009; Koch-Larrouy et al., 2015; Bouruet-Aubertot et al., 2018; Xu et al., 2020), or modeling results (e.g. Koch-Larrouy et al., 2007).

This crucial vertical eddy diffusivity close enough to the surface along the IT paths may play a role in modulating heat (e.g., Assene et al., 2024) and chlorophyll content (de Macedo et al., 2023; M'Hamdi et al., 2024; in preparation) observed off the Amazon shelf.

Our study also found the highest dissipation rates at stations S3 and S5 of [10^{-6},10^{-4}] W kg^{-1} on the Amazon shelf , increasing near the bottom boundary layer. These findings compare well with values reaching up to 10^{-9} W kg^{-1} within a kilometer of the seabed in the Southern Ocean (Sheen et al., 2013) and up to 10^{-6} W kg^{-1} within a few meters from bottom topography off the Changjiang Estuary (Yang et al. 2020). This may indicate the

presence of an active bottom boundary layer. Thus, kinetic energy of bottom flow was estimated using friction velocity, that was computed from total velocity averaged over the bottom-most 15 m for shallow stations. It showed bottom friction energy stronger between 16-35 J m^{-2} at S3 and S5 mainly and lower (< 3 J m^{-2}) in the other stations on shelf (e.g., at S8). These results are smaller but still important on the Amazon shelf and comparable to values (517 kJ m^{-2}) in the Drake Passage region (on the continental slope) of the Southern Ocean (Laurent et al., 2012). The bottom mixing at S3 and S5 can indirectly exert a control on pycnocline mixing on the Amazon shelf (Inall et al., 2021).

Contribution of Background circulation and ITs to mixing

Mean baroclinic current shear

Another important aspect addressed in this study was quantifying the contributions of different processes to the observed heterogeneous mixing.

First, the mean baroclinic current (BC) was considered as a proxy for the background circulation. The BC was predominantly structured into a northwestward surface flow and a southeastward subsurface flow along the IT pathways. The strong surface flow toward the northwest is associated with the North Brazil Current (NBC), which originates from the northeastern coast of Brazil (e.g., Bourlès et al., 1999) and propagates along the Amazon shelf-break (e.g., at stations S7, S10, S11, S14, and S24). Conversely, the southeastward subsurface flow observed at stations such as S7 and S11 might result from NBC instability or the presence of a countercurrent at depth (Dossa et al., 2024, in preparation). At site E, the flow reversal observed at S21 - characterized by a southeastward surface flow and a northwestward subsurface flow - was located inside of the outer path of the Amazon plume. This reversal could be related with the influence of AWL formed by continental inputs (Prestes et al., 2018).

Both baroclinic flows demonstrated a significant potential for shear instability, with vertical shear ranging from 10^{-5} to 10^{-3} s^{-2} off the Amazon shelf. The shear associated with the NBC was particularly pronounced around the pycnocline (between 40 and 200 m depth) at sites Aa, Ab, and G (e.g., at S6, S7, S10, S11, S14, and S24). At site E, the shear instability was stronger (> 2.5 x 10^{-4} s^{-2}) at the base of the pycnocline (e.g., at S20), potentially associated with NBC retroflection near [5–6°N, 50°W] during the fall season (Didden and Schott, 1993). The higher BC shear observed at S21, where flow direction reversals occurred, could be associated with the presence of a subsurface cyclonic eddy (Dossa et al., 2024, in preparation).

ITs shear

Second, the baroclinic tidal current was extracted from the total baroclinic current, revealing significant semi-diurnal (M2) component signals around the pycnocline. These signals, characterized by higher tidal modes (3-5), were more pronounced at generation and propagation sites Aa and Ab (e.g., at S6, S10, and S14) compared to other sites. The tidal shear within the pycnocline layer (80-120 m) is consistent with the observed IT signal patterns and large vertical displacements. It was stronger, reaching up to 10^{-3} s^{-2}, near the generation sites Aa and Ab (at S6 and S10) and in the open ocean at S14. Further from the generation sites (e.g., at S7, S11, and S20), the IT shear was smaller but still notable (reaching up to 10^{-4} s^{-2}). This highlights the significant role of ITs in driving mixing processes, particularly within the pycnocline, where strong vertical shears were

observed near the shelf-break compared to regions far away. Outside the IT fields, such as at S24, the persistent high vertical shear near the bottom topography could be attributed to the active bottom boundary layer (Inall et al., 2021).

IT/BC ratio

Both IT and BC shear contribute to mixing, with their relative dominance varying across sites. Near the generation sites on the shelf-break, IT shear dominated the IT/BC shear ratio, such as at S6 (61.44/38.56 %), S10 (65.82/34.18 %), and S21 (58.55/41.45 %). Along the IT paths, the contributions were nearly equal (~50/50 %) at locations farther from the generation sites (e.g., at S20, S7, S11, and S13), except at S14 in the open ocean, where IT shear remained dominant (58.50/41.50 %). These findings align with the presence of ITs at generation sites Aa, Ab, and E (Tchilibou et al., 2022; Assene et al., 2024) and the stronger energy associated with NBC cores, particularly at S7 and S11.

These results are consistent with previous studies that identified strong tidal shear near IT generation sites, such as the Halmahera Sea (Bouruet-Aubertot et al., 2018), the Changjiang Estuary (Yang et al., 2020), the northwest European continental shelf seas (Rippeth et al., 2005), and the southern Yellow Sea (Xu et al., 2020).

The most relevant finding of this study was the relative increase in mixing within the pycnocline layer, observed at S14 in the open ocean, far from the IT generation sites.

Discussion on the strong mixing at S14

Along the IT paths, elevated remote dissipation rates (within $[10^{-7}, 10^{-6}]$ W kg^{-1}) were identified ~ 230 km from the shelf-break at S14.

This region is well known for intense IT dissipation, as shown by a realistic model (Tchilibou et al., 2022; Assene et al., 2024), and for the highest occurrences of ISWs generated by ITs (Fig. 1a; de Macedo et al., 2023), with large-amplitude ISWs exceeding 100 m clearly visible in satellite records (Brandt et al., 2002).

At station S14, where relative mixing increases, IT rays surfacing from two distinct IT generation sites coincide with the appearance of ISWs and mark the location where the NBC vanishes.

This region of wave-wave interactions can lead to the constructive interference of IT rays, potentially facilitating the emergence of higher tidal modes (New & Pingree, 1992; Silva et al., 2015; Barbot et al., 2022; Solano et al., 2023). These higher modes, in turn, could enhance the generation of nonlinear ISWs (e.g., Jackson et al., 2012) and contribute to the elevated dissipation rates (Xie et al., 2013), as observed at this station.

Moreover, IT interactions with baroclinic eddies may also contribute to turbulent dissipation (Booth and Kamenkovich, 2008), particularly in this area of pronounced eddy activity. However, no repeated AMAZOMIX stations observed during a tidal period were enclosed by mesoscale eddy activity, except potentially around site E, where possible evidence of a subsurface eddy was detected at S21 (Dossa et al., 2024, in preparation).

Future studies are needed to unravel the intricate interplay among these processes. The data collected during the AMAZOMIX cruise will provide a guide for improving our understanding and advancing parameterizations for modeling studies.

"

As a conclusion, I think this manuscript is no ready for publication and needs significant work to produce convincing results. I think the most efficient way to proceed is a new submission.